Computer Modeling of Local Level Structures in (Ce, Zr) Mixed Oxide

José C. Conesa*

Instituto de Catálisis y Petroleoquímica, CSIC, Campus de Cantoblanco, 28049 Madrid, Spain

Received: January 3, 2003; In Final Form: May 6, 2003

Atomistic and quantum DFT calculations are carried out for models of $Ce_{0.5}Zr_{0.5}O_2$ mixed oxide having different cation orderings within a fluorite-type structure. The DFT results are more accurate than those given by the atomistic calculations; these latter exaggerate oxygen sublattice distortions and energy differences between different cation orderings. The results imply that using an "averaged cations" approach in atomistic simulations is likely to miss relevant effects of cation distribution details at local levels. The lowest energy is obtained with a double-layer type of cation clustering, in agreement with some EXAFS data; the typical tetragonal crystal cell distortion, however, is obtained optimally with a different, nonclustered scheelite-type ordering, similar to that of other related mixed oxides, which is also among the lowest energy structures obtained and agrees with other published EXAFS data. Implications of the predicted Zr−O coordination configurations for the interpretation of EXAFS data are discussed. The κ-phase, formed by controlled reoxidation of the $Ce_2Zr_2O_7$ pyrochlore so as to keep the same cation arrangement as in the latter, is effectively confirmed to be rather less stable, at least when defect-free. The DFT calculations predict for it a crystal symmetry lower than cubic but with almost exactly cubic unit cell dimensions; its discrepancies with the XRD-derived published crystal structure are discussed in connection with symmetry lowering effects and with the likelihood of the presence of anionic Frenkel defects. The possibility is discussed that this phase could have different surface acidity and XPS features (because of modified Ce ion charges) as well as a smaller band gap in agreement with some experimental observations.

Introduction

Cerium−zirconium mixed oxide (CZMO) has been the subject of extensive study in recent years mainly because of its high efficiency as oxygen buffer and promoter in the latest generation of the so-called three-way catalysts (TWCs) used for purifying automobile exhaust gases,[1,2,3] other applications such as its use as ionic conductor (e.g., in fuel cells)[4] or as active support in catalysts for reforming[5,6] or water gas shift reactions[7] being also of interest.

This oxide exists normally as a solid solution having a fluorite structure, that is, that of CeO_2 but with part of cerium substituted by zirconium, its composition being therefore describable as $Ce_{1-x}Zr_xO_{2-y}$ (where $y = 0$ corresponds to the fully oxidized state and $y > 0$ to a reduced state). In the fully oxidized state (the case considered in this work), in the absence of apparent cation ordering the cubic fluorite symmetry (space group $Fm\bar{3}m$) usually undergoes distortions. In particular, for $x \geq 0.4$, the stable configuration of CZMO has a tetragonal cell with $c/a > 1.00$; it is assumed that, as in tetragonal zirconia, the anions are displaced from the ideal tetragonal sites in directions parallel to the c axis in a way conforming to the space group $P4_2/nmc$. This is normally designated as t′ phase, although it has been indicated that several such tetragonal phases (named t′, t*, t_{meta}, and so forth) may appear in preparations made under different conditions at moderate or high temperature; these phases, which might differ in lattice distortions or ion-ordering details, would be distinguishable mainly through thermodynamic properties and Raman spectra, while their diffraction features would be nearly the same.[8,9,10] It is also known that, for $0.4 > x > 0.2$, one may have a perfectly cubic cell shape ($c/a = 1.000$) while still having displaced oxygen anions; these displacements imply a decreased symmetry which manifests itself in the presence of several peaks in the Raman spectrum, typically four, while the truly tetragonal lattice presents six peaks and the undistorted fluorite lattice would allow only one. This is designated normally as the t″ phase[9,11] and may occur also for compositions up to ca. $x = 0.50$ if the crystallite size is small,[3] as frequently happens in catalyst materials. It is presumed that in this t″ phase, the anion displacement pattern still conforms to the $P4_2/nmc$ tetragonal group, and indeed high precision X-ray and neutron diffraction profiles have recently been fitted successfully within it;[9] however, in one case[12] convergent beam electron diffraction data obtained for a (doped) cubic zirconia specimen, which could be presumed to correspond also to a t″-type phase, have been interpreted in terms of a primitive cubic lattice of $P\bar{4}3m$ space group symmetry in which the displacements of the anions occur along the main diagonals of the cubic unit cell.

In all these studies, the CZMO is described as a random solid solution of ceria and zirconia, without considering any effects which may arise from specific distributions of the Ce and Zr ions; only in a few cases has the cation distribution or ordering been addressed. Particularly interesting is the situation with $x = 0.5$, which has been widely studied as it develops optimally the ion mobility properties relevant for the oxygen buffering effects in TWCs.[3] It is known[10,13,14] that upon reduction of a CZMO of this composition at high temperature, so as to achieve a $Ce_2Zr_2O_7$ stoichiometry, ordering of both cations and the produced anion vacancies occurs within the overall fluorite-type lattice (first hints of this occurring at 1123 K, the process being completed at 1573 K); this ultimately results in the cubic pyrochlore structure which has again an fcc lattice (now with

* Telephone: 34-915854766; fax: 34-915854760; e-mail: jcconesa@icp.csic.es.

10.1021/jp0340156 CCC: $25.00
Published on Web 07/19/2003

unit cell dimensions approximately twice those of the parent fluorite lattice) and symmetry corresponding to the $Fd\bar{3}m$ space group. In this case, the atomic ordering is such that each Ce ion, now in the Ce^{3+} state, remains coordinated to eight oxygen anions while Zr, remaining as Zr^{4+}, is six-coordinated; each one of the anion vacancies, which are ordered according to a diamond-type lattice, is then surrounded exclusively by Zr ions. If such reduced material is reoxidized at a more moderate temperature (e.g., at 850−1200 K), a fully oxidized solid results in which the lattice remains cubic and keeps the above-mentioned cell size doubling (this has been in fact related with periodicity doublings observed in high-resolution electron microscopy studies on this type of materials[15,16]); such structure has been designated as κ-phase.[17] It is presumed that here the anion vacancies are replenished with oxygen while the cations, which have low ion mobility at these temperatures, remain at the positions of the pyrochlore structure. Recent X-ray diffraction work confirms this picture but suggests that the crystal symmetry conforms rather to the (still cubic) $P2_13$ space group.[18] This situation is metastable in respect to a reordering (or disordering) of the cations, which takes place at temperatures of ca. 1300 K or above, when cation mobility becomes important enough, to give a tetragonal phase.[17] If the reoxidation of the reduced pyrochlore phase is carried out at a relatively mild temperature (e.g., 700 K), at which anion mobility itself may be limited, neutron diffraction studies[13,19] show that, even if the overall reoxidation of the material is complete, part of the tetrahedral anion sites remain unoccupied because the corresponding oxygen ions lie at interstitial positions (mainly around the octahedral voids of the fcc cation lattice), that is, anionic Frenkel defects are present. Detailed X-ray and neutron diffraction work allowed to determine space group (rombohedral $R\bar{3}m$) and (partially disordered) oxygen atom positions for one such situation.[20] Such interstitial oxygens, detected also in the similar Ce, Sn mixed oxide,[21] have been reported to remain in CZMOs even after oxidation at $T = 1050$ K, while in CeO_2 they would disappear above 900 K.[22]

While these cubic/tetragonal lattice transformations have been more or less extensively characterized, little is known with certainty, except in the mentioned κ and pyrochlore phases, on the relative disposition of both cations in the lattice and on its dependence on synthesis and physicochemical treatment conditions. Cation-ordering effects may be, however, relevant. Indeed, there is an important degree of metastability in at least some of the mentioned tetragonal phases, so that handling them in oxidizing environments at temperatures of ca. 1400 K and above may lead, if appropriate nucleation conditions exist, to disproportionation into two separate CZMO phases which are, respectively, richer and poorer in Zr than the parent material.[23] Most important of all, high-temperature oxidation/reduction cycles, carried out on these materials in conditions appropriate for producing cation rearrangements, may lead to very different rates of oxygen uptake and release at moderate temperatures,[24,25] this being the key parameter for a good oxygen buffering efficiency in TWCs. The reason for this behavior has not yet been elucidated, but the temperatures leading to these changes lie in the range appropriate for cation migration and reordering, so it seems natural to ascribe this effect to changes in the relative distribution of both cations. Spectroscopic data indicate that there may be in these situations a subtle interplay of bulk and surface atomic rearrangements.[26]

In this respect, EXAFS works by several groups give indications of various types of cation arrangements. Thus, results obtained by Nagai et al.[27] (including spectra at the Ce K edge) for an apparently homogeneous $Ce_{0.5}Zr_{0.5}O_2$ material of high surface area (and therefore low crystallite size) prepared by coprecipitation have shown that the relative ordering of cations is such that the average numbers of Ce and Zr nearest cation neighbors around each Ce ion are, respectively, $N_{CeCe} = 8$ and $N_{CeZr} = 4$ Zr (and, conversely, the number N_{ZrCe} of Ce neighbors around each Zr ion is $N_{ZrCe} = 4$), that is, this material would have some sort of Ce−Ce and Zr−Zr clustering, while similar measurements for the κ-phase made in the same study show, as expected, a (6 Ce + 6 Zr) neighbor configuration around each cation. Quite an opposite observation has been reported in another study on materials of approximately $Ce_3Zr_2O_{10}$ composition subjected to relatively high-temperature treatments:[28] the N_{ZrZr} values are lower (and N_{ZrCe} higher) than those corresponding to random cation distribution.

Despite the relevance that, in view of these observations, the mutual arrangement of cations in CZMO must have in determining key properties of this material, many fundamental studies describe it just as a random solid-state solution. Indeed, computer simulations appeared in recent years use an "averaged cation" description,[29,30,31] and the anion coordination around Zr discussed in recent EXAFS work[32] is based on a description of the structure within the above-mentioned $P4_2/nmc$ space group, which implies not only the equivalence of all cations but also of all anions (so that arguing within this context, as done in ref 32, that there are two types of oxygens with different bond strength and ease of elimination is not appropriate). It seems therefore convenient to make efforts to understand the characteristics of $Ce_{0.5}Zr_{0.5}O_2$ materials considering the specific mutual distribution or ordering of the cations that may be present in them. Computer simulation work in this direction is presented here, trying to relate several different cation orderings with the ionic displacements and lattice distortions induced by them and their energetic consequences and examining also possible effects on their electronic structures. It was expected that during this exercise regularities would emerge that could allow to relate some of the experimental observations to specific atomic configurations and thus to obtain a better insight on the factors which control at an atomic scale their most relevant properties.

Computational Methods

Atomistic calculations (geometry optimizations and lattice energy evaluations) were carried out for all structures using the GULP code,[33] version 1.3. As done in previous works,[29,34] besides the Coulomb interactions (which were computed using Ewald sums[35] and assuming formal charges for all ions), short-range interactions were modeled with the Buckingham potential, formed by a repulsive (Born-type) exponential term and an attractive C/r^6 term which represents dispersion interactions. For all three elements involved, polarizability effects were taken into account using the shell model,[36] which represents each ion as formed by an atomic core and a rigid, massless spherical shell mutually linked by a harmonic potential. The parameters for all these energy terms were taken from the literature.[29] Starting from structures constructed as explained below, the corresponding unit cell dimensions and the ions' positions within them were simultaneously relaxed with GULP until the energy minimum was obtained. In principle, full use of symmetry is made for improving computational speed. This implies that relaxations are carried out within the constraints of the symmetry specified, thus forbidding spontaneous departure from it. Any tendency to symmetry decrease (within the same primitive cell) was checked by computing subsequently, through diagonalization of the dynamic matrix, the phonon frequencies at the

Γ-point (Brillouin zone center); whenever negative values were obtained, indicating that the configuration corresponded to a saddle point in the energy hypersurface, the symmetry was lowered by applying atom displacements following the normal modes corresponding to those negative frequencies, and the configuration was reoptimized until these latter disappeared. Additionally, tendencies to a further spontaneous symmetry decrease with formation of supercells (and doubling or tripling of cell parameters) were checked by computing phonon frequencies at other special points of the Brillouin zone (BZ) with some coordinates equal to 1/2 or 1/3. When negative frequencies appeared, supercells with doubled or tripled cell parameters were built, by which procedure these special points were folded into the Γ-point, and then the distortions eliminating the negative frequencies were determined as above. The final symmetry of the structures was determined using the *Find_symmetry* tools of the Cerius2 suite (version 4.2) of molecular and solid modeling programs.[37]

Several of the thus obtained structures (see Results section below) were subjected to reoptimization and energy evaluation using self-consistent quantum chemical calculations within a density functional theory (DFT) approach. These calculations were carried out using the total energy CASTEP code, as implemented in Cerius2. This code uses a plane wave description of the periodic single-electron wave functions (i.e., a Fourier expansion),[38] the atomic cores (1s for O and up to Zr 3spd and Ce 4spd shells for the heavier atoms) being represented by pseudopotentials of the ultrasoft Vanderbilt type[39] derived from relativistic atomic computations. Geometry reoptimizations and density-of-state (DOS) calculations were carried out within the local density approximation (LDA, with the Perdew−Zunger parametrization[40]) and using a plane wave cutoff of moderate precision (330 eV, the "medium" cutoff setting in CASTEP for this type of system). For the thus refined structures, final and more accurate energy values were then computed with the same code using a higher cutoff value (410 eV, the "precise" cutoff) and the generalized gradient approximation (GGA) as specified by Perdew and Wang.[41] In both stages of DFT calculations, an energy correction for the finite character of the plane wave basis set[42] was included. Also, full use of symmetry was made; this allows to carry out the calculations including only nonequivalent points in the **k** space grid used for sampling the BZ. This grid, designed according to a Monkhorst−Plank (MP) scheme, was chosen so as to contain at least 4−6 nonequivalent points and to give a sampling interval of not more than 0.05−0.06 $Å^{-1}$. Phonon frequency calculations are here computationally too expensive and were not carried out; it is expected that any residual tendency to symmetry breaking not foreseen by GULP will be of only marginal importance (at least for the purposes of the present work) and without any significant effect on the obtained energies and basic geometric properties of the structures obtained. Indeed, the results obtained (see below) show that the DFT calculations tend to predict structures less distorted than those given by the atomistic ones.

From the electronic structures obtained in the DFT calculations, data were obtained about the electron density distribution in the different constituent atoms. This was achieved following a method,[43,44] available in the CASTEP−Cerius2 package, in which the periodic single-electron orbital functions are projected into atomic orbitals generated independently with a high-precision atomic program, so that those periodic orbitals can be described as combinations of atomic contributions. This decomposition, although not exact, constitutes a rather good approximation, as checked with the "spilling factor" (percentage of the total electron density that cannot be captured in this decomposition),[44] which in the present study was in almost all cases below 1%. In this way, a Mulliken-type population analysis can be carried out.

Models Examined. Several models of $Ce_{0.5}Zr_{0.5}O_2$ were built by locating in the cation sites of the CeO_2 fluorite structure Ce and Zr ions according to different orderings, which included all order topologies known in ABO_2 oxides of rocksalt structure[45] (where necessary, supercells were constructed so as to have in all cases initially eight cations per unit cell to homogeneize the accuracy and flexibility to distortions):

(1) Alternating single planes of Ce and Zr, oriented parallel to the (100) plane of the parent fluorite; this layered topology, which is equivalent to that of alternating single-cation planes parallel to the fluorite (110) plane, is labeled here as **l**. This is the ordering which results when one starts from the tetragonal lattice with $P4_2/nmc$ symmetry with which CZMOs are frequently described and then forces the two cations in its unit cell to become inequivalent (i.e., one Ce and one Zr). In this case, the symmetry decreases (initially) to the $P\bar{4}m2$ space group and two inequivalent types of anion appear.

(2) Alternating single Ce and Zr planes parallel to the fluorite (111) plane, resulting in a topology of initially rombohedral symmetry; this is labeled **r**. This coincides with the cation ordering in α-$NaFeO_2$ and with that proposed for the well-crystallized material examined with EXAFS in ref 46.

(3) Alternating double Ce and Zr planes, parallel to (100) (labeled **d**), (110) (labeled **i**), or (111) (labeled **b**). The **i** case coincides with the cation ordering in β-$NaMnO_2$.

(4) The same cation ordering reported to exist in the κ-phase of $CeZrO_4$, that is, that existing in the pyrochlore structure; this is labeled **k**. It coincides with the ordering in $Li_2Ti_2O_4$.

(5) The same ordering as in the scheelite-type oxides $CeGeO_4$, $ThGeO_4$, $HfGeO_4$,[47,48] and $LaNbO_4$;[49] this is labeled **s**. It coincides with the ordering in γ-$LiFeO_2$.

(6) A tetragonal lattice resulting from arranging, in a checkerboard pattern parallel to the *ab* plane, fluorite unit cells containing only Zr or only Ce cations, and repeating this along the *c* axis so as to form Zr-only and Ce-only columns; this is labeled **c**.

(7) The relatively complex cation ordering present in β-$LiFeO_2$, where each cation type sublattice presents alternating narrow, parallel ribbons of (111) planes. This is labeled **f**.

(8) Other structures with some degree of symmetry which result from mutually exchanging one-quarter of the Ce and Zr atoms in some of the lattices described above. Structures appearing in this way are labeled **m** (formed from **s** by exchanging cations in the $z = 0.5$ plane of the tetragonal cell), **t** (from **c**), **u**, **v**, **w**, **x** (from **d**), **y** (from **r**), and **z** (from **l**).

In general, as said above configurations specifying eight cations per primitive cell were sought initially. In some of the simplest structures, when the topology of the cation arrangement leads to small primitive cells, multiples of these were constructed manually, leading to different primitive lattice and symmetry specifications; this allowed to identify in some cases, after the relaxation process, more than one (local) energy minimum for a given type of cation-ordering topology. For the κ-phase topology, two structures were used as alternative starting points: a regular fluorite lattice with ordered cations (i.e., as in the rest of the cases) and the structure derived for this phase from diffraction data,[18] once distorted to another one without symmetry using eigenvectors of imaginary phonon frequencies determined with GULP. To better identify the different structures, in what follows the standard number of the space group

TABLE 1: Excess Energy ΔE and Relative Molar Volume V_{rel} (in Comparison with the Combination $^1/_2ZrO_2$(M) + $^1/_2CeO_2$), and Number of Cations Per Primitive Unit Cell, Resulting from Computations with Programs GULP and CASTEP for Different $Ce_{0.5}Zr_{0.5}O_2$ Structures; the Number N_{MM} of Similar Cation Neighbors Is Also Displayed. ΔE and V_{Rel} Values Computed for Tetragonal ZrO_2, as Compared with the Monoclinic Form, Are Given in the Lower Part of the Table

			ΔE (kJ/mol)		V_{rel}	
structure[a]	N_{MM}	N_{cat}/p.c.	GULP	CASTEP	GULP	CASTEP
r2	6	12	23.77		0.9681	
r4(→**r**166)[b]	6	16 (→2)	23.01	19.63	0.9749	0.9622
k19(→**k**62)	6	16	21.02	22.63	0.9886	0.9618
(**k**146)[c]	6	32		21.68		0.9660
i2(→**i**11)	6	12 (→4)	20.68	15.46	0.9777	0.9688
y4(→**y**55)	6	16	19.97	20.29	0.9840	0.9671
b5 (→**b**11)	9	32 (→8)	18.73	13.56	0.9893	0.9757
f2	5	8	17.60	16.90	0.9803	0.9881
z5	5	8	16.70		0.9838	
x4	6	16	16.11		0.9893	
w18	6	16	14.48	18.18	0.9985	1.0069
u4	6	8	14.45		0.9999	
t3	5	8	14.26		0.9839	
v3(→**v**16)	6	8	12.50	20.08	0.9973	0.9862
c138	6	16	11.87	15.39	0.9924	0.9876
l130	4	16	10.38	17.95	0.9875	0.9833
d7	8	16	9.13	11.20	0.9977	0.9934
s88	4	4	7.19	15.43	0.9982	0.9836
m122	4	8	7.11	23.14	0.9911	0.9815
l125	4	4	5.51	20.19	0.9891	0.9855
d29	8	8	5.37	11.47	1.0050	1.0095
d45	8	8	−11.71	11.05	1.0100	0.9963
ZrO_2 (tetr)	12	2	15.92	13.10	0.9381	0.9534

[a] The number (no.) in the label indicates the space group. Cases with 142 > no. > 74 are tetragonal; monoclinic ones have no.< 15, while no. = 146 and 166 are rombohedral. [b] Indications such as (→*x*) mean cases where the symmetry increases (and N_{cat}/p.c. possibly decreases) when optimizing with CASTEP the structure found with GULP. [c] Results obtained with CASTEP starting from the published κ phase structure[18] (see text).

determined in each case will be appended to the one-letter label (**l**, **r**, **d**, etc.) used as said above to specify the cation-ordering topology.

Results

All the above-mentioned structures were first subjected to relaxation with GULP. In most cases, the structures relaxed within the maximum (topological) symmetry had imaginary frequency phonon modes at the Γ-point, and in nearly half of them also at other special points in the Brillouin zone, so that a symmetry decrease (and eventually supercell generation) followed by reoptimization, as explained above, was required. The lattice energies obtained are expressed as the energy change ΔE (per mol of MO_2) corresponding to the reaction

$$^1/_2\ CeO_2 + {}^1/_2\ ZrO_2 \rightarrow Ce_{0.5}Zr_{0.5}O_2$$

where the data for the single oxides (taking for zirconia those of the monoclinic phase) were computed by the same method. These GULP-derived ΔE values are summarized, in ascending order, in Table 1, which includes also the molar volume of the mixed oxide lattice (relative to the average of the values computed for ceria and monoclinic zirconia) and the number of cations per primitive cell which results in each case after the symmetry lowerings required. For the **k** cation ordering, both starting structures used (see above) led in the GULP calculations to the same final relaxed structure (**k**19, orthorhombic). Table 1 also gives the average number N_{MM} of Ce(Zr) cations in the nearest cation coordination shell around a Ce(Zr) ion; for this composition, $N_{CeCe} = N_{ZrZr}$, $N_{CeZr} = N_{ZrCe}$, and $N_{MM} + N_{MM'} = 12$ (where M ≠ M′). For comparison purposes, the value obtained for the energy difference found between the tetragonal and monoclinic ZrO_2 forms is also included in Table 1. Table 2 summarizes the main geometric parameters, computed and experimentally determined, of the single oxide lattices and of some $Ce_{0.5}Zr_{0.5}O_2$ materials characterized in the literature.[50−52,18,10]

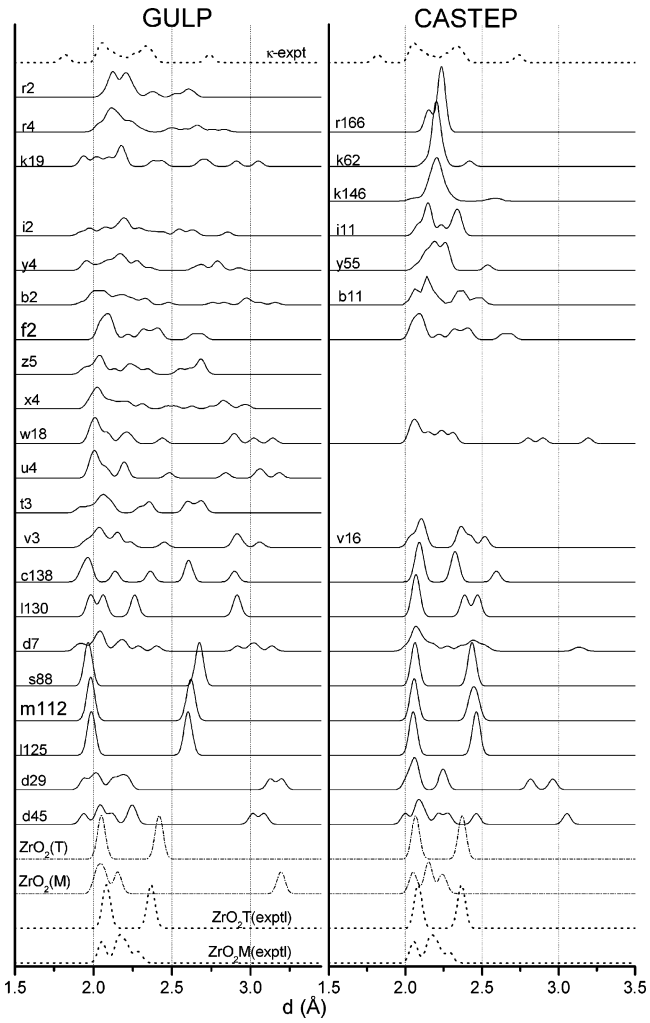

Figure 1. Radial distribution function plots for the Zr−O atom pair (broadened with a Gaussian of 0.03 Å width) as computed by the atomistic (GULP) and DFT (CASTEP) methods for several $Ce_{0.5}Zr_{0.5}O_2$ structures (ordered according to the energies obtained with GULP) and for the tetragonal and monoclinic ZrO_2 lattices. For comparison, dotted line plots corresponding to experimental structures are included: in the lower part, for ZrO_2; in the upper part, for the structure reported for the κ phase.[18] Labels indicate both the cation distribution topology and the space group obtained after relaxation (see text).

In all these structures, the oxygen coordination around Zr was examined; it is presented in Figure 1 in form of averaged radial distribution function (RDF) of O ions around Zr at distances up to 3.5 Å, convoluted with a Gaussian profile of 0.03 Å width. The same figure presents the corresponding RDFs computed for the monoclinic and tetragonal ZrO_2 forms (also relaxed, but obviously without allowing cell volume doubling in the latter) as well as those corresponding to these two structures as experimentally determined. In addition, the upper part of the figure includes the Zr−O RDF corresponding to the cubic structure derived for the κ-phase from diffraction data[18] (in particular, for the second structure presented and preferred

TABLE 2: Crystal Structure Data Computed with GULP and CASTEP for Single Ce and Zr Oxides and for Some Experimentally Characterized CZMO Structures[e]

structure	parameter	GULP	CASTEP	exptl
CeO_2	a	5.429 Å	5.398 Å	5.4112 Å
ZrO_2 (mon)	a	5.241 Å	5.111 Å	5.169 Å
	b	4.898 Å	5.186 Å	5.232 Å
	c	5.579 Å	5.275 Å	5.341 Å
	b	89.999°	99.54°	99.25°
	vol/MO_2	35.804 Å^3	34.472 Å^3	35.641 Å^3
ZrO_2 (tetr)[a]	a	3.588 Å	3.561 Å	3.598 Å
	c	5.218 Å	5.186 Å	5.152 Å
	Δx(O)	0.060	0.049	0.040
	c/a	1.0283	1.0299	1.0180
	vol/MO_2 (V_{rel})	33.586 Å^3 (0.9381)	32.875 Å^3 (0.9534)	33.348 Å^3 (0.9357)
κ-$Ce_{0.5}Zr_{0.5}O_2$[b]	vol/MO_2[d] (V_{rel})	37.486 Å^3 (0.9888)	35.488 Å^3 (0.9617)	36.456 Å^3 (0.9689)
t-$Ce_{0.5}Zr_{0.5}O_2$[c]	a	3.739 Å	3.703 Å	3.720 Å
	c	5.288 Å	5.237 Å	5.260 Å
	c/a	1.0236	1.0107	1.009
	vol/MO_2 (V_{rel})	37.848 Å^3 (0.9984)	36.291 Å^3 (0.9835)	36.715 Å^3 (0.9758)

[a] Reference 52. [b] Reference 18. [c] Reference 10 (with the *a* and *c* values appropriate to the tetragonal cell with 2 cations/unit cell, for better comparison with simulation). [d] The GULP and CASTEP results refer to the **k**19 and **k**146 structures, respectively. [e] The computed data presented for the t′-phase are those of the **s**88 structure, which is the only tetragonal one appearing with correct *c*/*a* ratio and low energy.

as more likely in that work). This type of data presentation provides a good visual impression of the extent of local structure distortion introduced by the lower radius of the Zr ion combined with its specific ordering.

For all of the ordered ceria−zirconia structures mentioned within no. 1−7 in the Models Examined section above and for a few of the others mentioned in no. 8 as well as for the single oxides, starting from the corresponding GULP-relaxed configurations DFT calculations were made with the CASTEP code, carrying out with the latter new geometry optimizations and total energy evaluations. The ΔE and V_{rel} values thus obtained are given in Table 1, and the RDFs of O ions around the Zr cations are given in Figure 1; the relevant geometric parameters are presented in Table 2. In several cases, indicated through the different space group number in Table 1 and Figure 1, the structure resulting was more symmetric than that which had been predicted by GULP (and which was the starting point for the relaxation with CASTEP); this happened almost exclusively for topologies which yielded relatively high energies in the GULP calculations. The number of atoms per unit cell, however, was affected (decreased) only in a few cases. In the **k** case, an optimization with CASTEP carried out starting directly from the structure published by Kishimoto et al.[18] (but with atomic positions slightly displaced according to negative frequency eigenmodes, as said above) led to a structure of rombohedral symmetry (**k**146, space group *R*3) different from the orthorhombic one (**k**62**)** obtained starting from the fully GULP-optimized one. A plot facilitating a visual comparison between the ΔE values obtained through both methods is presented in Figure 2. Pictorial representations of some of the most significant structures obtained, qualitatively visualizing the magnitude of the atomic displacements resulting after relaxation, are given in Figure 3. Since, as explained below, the DFT method can be considered as more reliable (even if computationally much more expensive) than the atomistic one, the rest of the data presented from now on correspond to the results of these DFT calculations, paying attention mainly to the most significant structures (those with lowest energies or simple orderings or serving as model of the κ phase). In particular, Figure 4 displays the RDFs obtained in them (and also that computed for the XRD-based structure reported for the κ-phase[18]) for all ion pairs except O−O. All the structures optimized with CASTEP are available separately as Supporting Information.

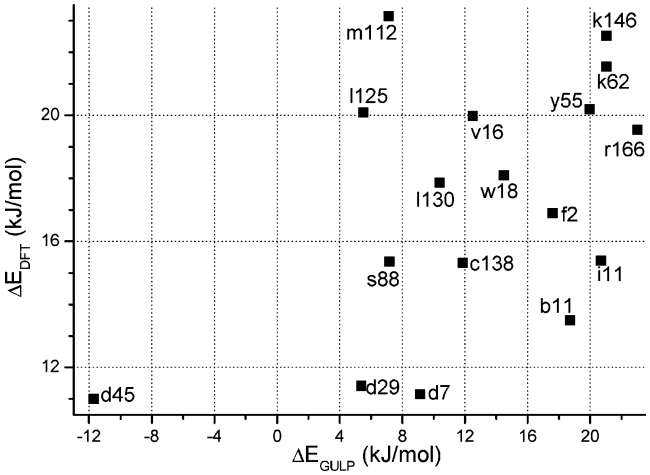

Figure 2. Comparison of ΔE values obtained with DFT calculations (ordinate axis) with those obtained with the atomistic method (abscissa axis).

The structures obtained have almost always a symmetry lower than the maximum possible one within the corresponding cation-ordering topology; in the majority of cases, they are distorted to orthorhombic or even monoclinic symmetry. To visualize the degree of noncubic character in the unit cell shape, the powder X-ray diffractograms have been simulated for the structures optimized with CASTEP, and in Figure 5 the region around $2\theta = 58°$, corresponding to the (311) reflection in the parent fluorite structure, is presented for the main ones. For comparison, this figure presents also the simulated diffraction peaks corresponding to a disordered $Ce_{0.5}Zr_{0.5}O_2$ material with tetragonal symmetry and same cell dimensions as experimentally determined for a typical t′ phase.[10] A further comparison of XRD profiles can be made between those obtained for the **k** models and those simulated using the crystalline structures derived for κ phase-type materials on the basis of X-ray and neutron diffractograms in, respectively, refs 18 and 20 (where in the latter case anion Frenkel defects were found). This comparison, presented in Figure 6, shows that the peaks forbidden in the perfect pyrochlore-type structure, arising from a lower crystal symmetry, have in the preferred **k**146 model (case b, which was computed using thermal parameters similar to those of case c) an average magnitude similar to that resulting from the two

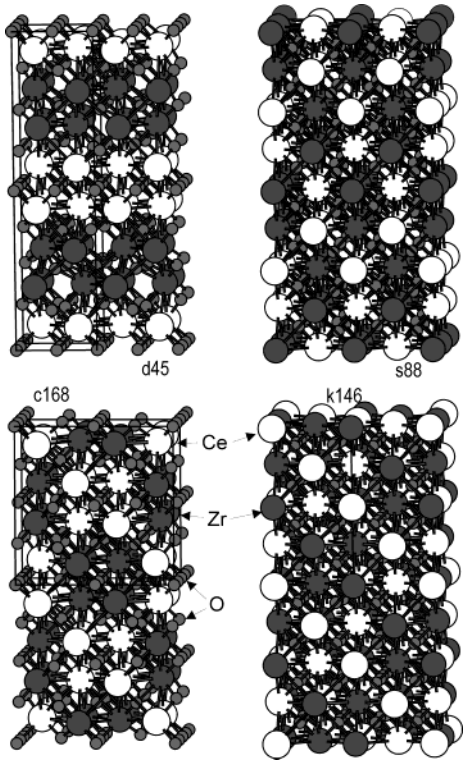

Figure 3. Representation of the lattices, as obtained after relaxation with the DFT method, for some of the most significant $Ce_{0.5}Zr_{0.5}O_2$ structures studied.

experimentally derived structures, while the relative intensities vary among these three cases.

Finally, the electronic structure information obtained with the DFT calculations (after lattice relaxation with this method) was examined. In the Mulliken population analysis, the results were relatively similar for all the $Ce_{0.5}Zr_{0.5}O_2$ structures: Zr ions presented Mulliken charges in the 1.24−1.33 range, with an electron density delocalization into the Zr 4d orbitals (which would be empty in the formal Zr^{4+} description) equivalent to 1.91−2.00 electrons; Mulliken charges of the oxygen ions were within the range −0.64 to −0.77. The largest variations in these parameters were observed for the Ce ions: although in the majority of cases their Mulliken charges appeared in the range 1.34−1.49, evidencing as expected a more ionic character for Ce than for Zr ions, and the electron densities in the 4f and 5d levels (empty in the formal Ce^{4+} description) amounted to 0.85−0.93 and 1.47−1.53 electrons, respectively; in a few cases (structures **l**130 and **k**62, but not so much in **k**146), the cerium Mulliken charges raised to values of 1.64−1.66. This latter change was due mainly to a lower amount of electron density in the 4f level, which corresponded then to 0.69−0.72 electrons. The **s**88 and **i**11 structures presented values more or less intermediate between those two situations, but here the values are less reliable since the spilling factor appears somewhat too high (ca. 2.4% and 3.2%, respectively), which means that in those cases the atomic orbital projection method used in the analysis captures less efficiently the electron density distribution. All these data can be compared with the results obtained for the single oxides: for both ZrO_2 forms, anion and cation Mulliken charges are ca. −0.72 and +1.44, respectively, and Zr 4d populations ca. 1.95; for CeO_2, charges are −0.63 and +1.27, and the electron densities at the Ce 4f/5d levels amount to 0.94/1.48. Comparison of these charge values with those given for the mixed oxide phases indicates that in these latter Ce and Zr are, respectively, more and less ionic than in their corresponding single oxides.

The main significant results concerning the energy positions of the different electronic levels, as obtained in these DFT calculations, are summarized with the density of state (DOS) plots presented in Figure 7. Although it is customary to present this type of data aligning the energy scale of each DOS with the others so that the top of the valence band coincides, examination of the positions of the other levels revealed inconsistencies if this criterion was followed. The most congruent results were obtained by aligning at the same energy (set here at ca. −47.25 eV below the top of the valence band) the center of the Zr(4s) level; then the energy scale of the CeO_2 DOS was aligned with that of the other structures on the basis of the position of the band gap edges. In this figure, only the lowest edge is displayed for the conduction band; the shape of the band itself was not considered of interest, and consequently to decrease the computational work only the four to six lowest empty orbitals, enough to define the position of that edge, were included in the calculation.

For most of the ceria−zirconia structures, these graphs show a valence band (presumably formed mainly by 2d orbitals of the O atoms) with a width of ca. 4.5−5.0 eV and a band gap of ca. 2.0 eV. The latter is relatively similar to that computed for CeO_2, while for ZrO_2 the conduction band lies significantly higher in energy (at a position, in the scale of Figure 7, of ca. 3.5/4.0 eV for the tetragonal/monoclinic forms), which clearly indicates that in the mixed oxides the bottom of the conduction band is formed mainly by Ce-based orbitals (of 4f type), in agreement with the conclusions from experimental data and other theoretical calculations.[53] One observes also that in the mixed oxides the position of the valence band bottom is more similar to that of ZrO_2 than to that of CeO_2. For the **k** structures, the band gap is appreciably narrower than in the other cases; a similar thing, although to a smaller extent, happens for the **r**166 structure that also has relatively high total energy and valence band edge position as shown in Table 1 and Figure 7, respectively.

Of the other electron levels accessible in these calculations, Figure 7 displays the DOS for the Ce(5s) and Zr(4p) states. For the Ce(5s) level only some shifts are appreciated, which cannot be taken as intrinsically very significant since the use of the Zr(4s) level as reference is somewhat arbitrary. In the Zr(4p) level, a certain degree of structure is observed; comparison with Table 1 soon reveals that the magnitude of the energy range spanned by this electronic level is clearly correlated with the number N_{ZrZr} of nearest equal neighbors, this range being wider for the pure ZrO_2 phases in which this number is the maximum possible (12). The range between −10 and −20 eV, where the Ce(5p) and O(2s) levels overlap and in which the DOS curves appear relatively unstructured and uninformative, is not displayed.

Discussion

Atomistic versus DFT Calculations. First of all, a comparison between the results obtained with the atomistic and DFT methods is in order. Concerning structural predictions, relevant indications are provided by the RDF plots in Figure 1. The RDFs of the two main experimentally known ZrO_2 phases are much better reproduced by the DFT calculation than by the atomistic

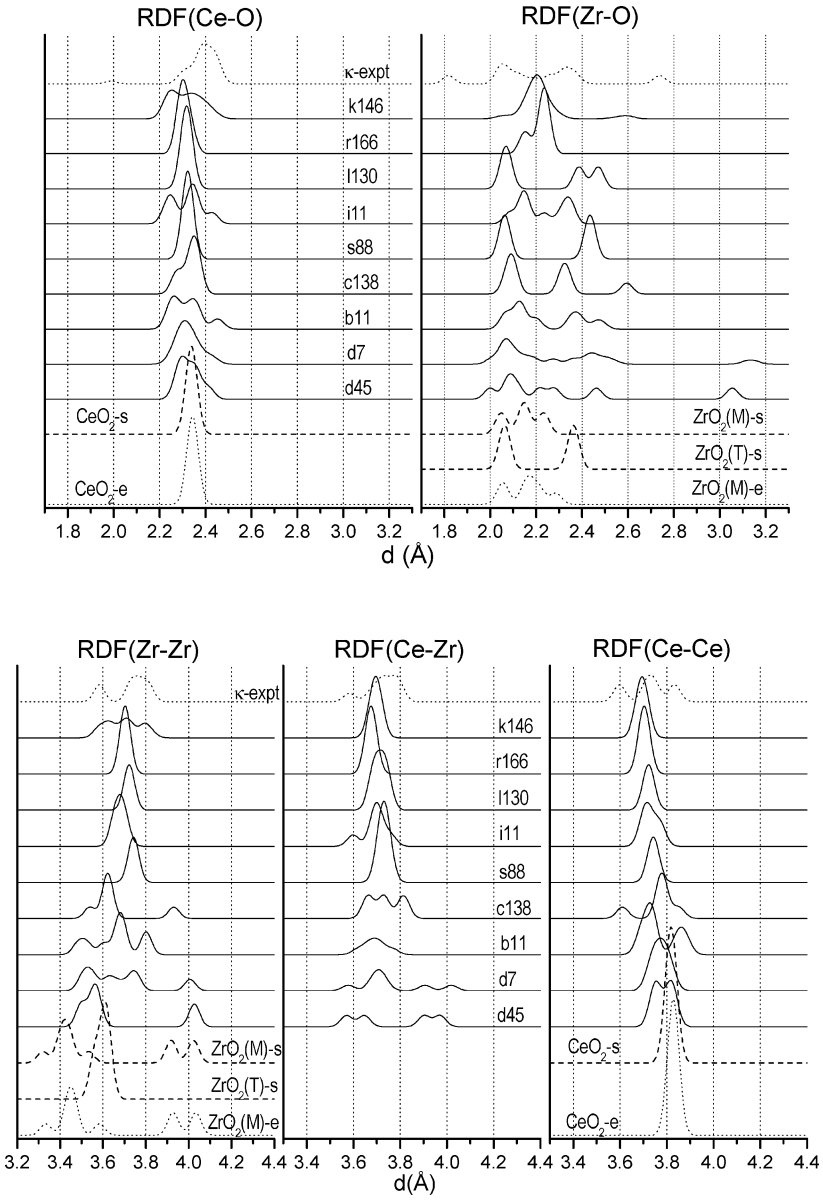

Figure 4. RDFs for all ion pairs except O−O (broadened with a Gaussian of 0.03 Å width) in the most significant DFT-relaxed CZMO structures studied, ordered according to the corresponding DFT energies. For comparison, plots corresponding to the structure proposed for the κ phase from experimental XRD data[18] are included also in the upper part and others corresponding to the pure oxides (simulated: dashed lines; experimental: dotted lines) are given in the lower part.

one. The spread in Zr−O distances is computed too high by the latter method in both lattices (the same trend appears when comparing the obtained results for all those CZMO structures in which both calculation methods have been used). Indeed, Table 2 shows that of the relevant geometric parameters only the tetragonal-to-monoclinic molar volume ratio is better reproduced by the atomistic calculation, while the cell shape of the monoclinic form is rather badly reproduced. At this point, one could try to use also the RDF plot derived from the experimental structural data reported for the κ-phase[18] (also included in Figure 1 for completeness) to compare it with those computed by both methods for the corresponding **k**-type structure. However, these experiment-based data must be used with caution, since as commented in detail below they conflict with EXAFS data obtained for the same phase[27] and there are uncertainties concerning the possible existence of defects in the structure. For this reason, here it is not considered safe to use these XRD-derived data to ascertain the reliability of the calculation methods.

In addition, the value obtained for the difference in energy between both ZrO_2 structures (13.1 kJ/mol), given in Table 1, can be considered. To this author's knowledge, there is in the literature no experimental data about the difference in energy between these two forms either at ca. 0 K (the temperature to which all these simulations correspond, as they do not include thermal vibration contributions) or at room temperature. One may, however, get some hint from the values in the NIST-JANAF tables.[54] According to these, at the transition temperature of 1478 K the heat of the monoclinic to tetragonal transition is 5.94 kJ/ mol, and the heat capacities C_p of the monoclinic and tetragonal forms are 80.108 and 74.45 J/K.mol, respectively; this latter difference in C_p means that the difference in enthalpy between both forms will be larger at lower temperature. If the difference ΔC_p between the C_p values remained constant all the way down to 0 K, at this latter temperature the difference in enthalpy would become 14.3 kJ/mol. This is necessarily an upper limit value, since both C_p values, and hence ΔC_p, will tend to zero when approaching 0 K; as a more realistic

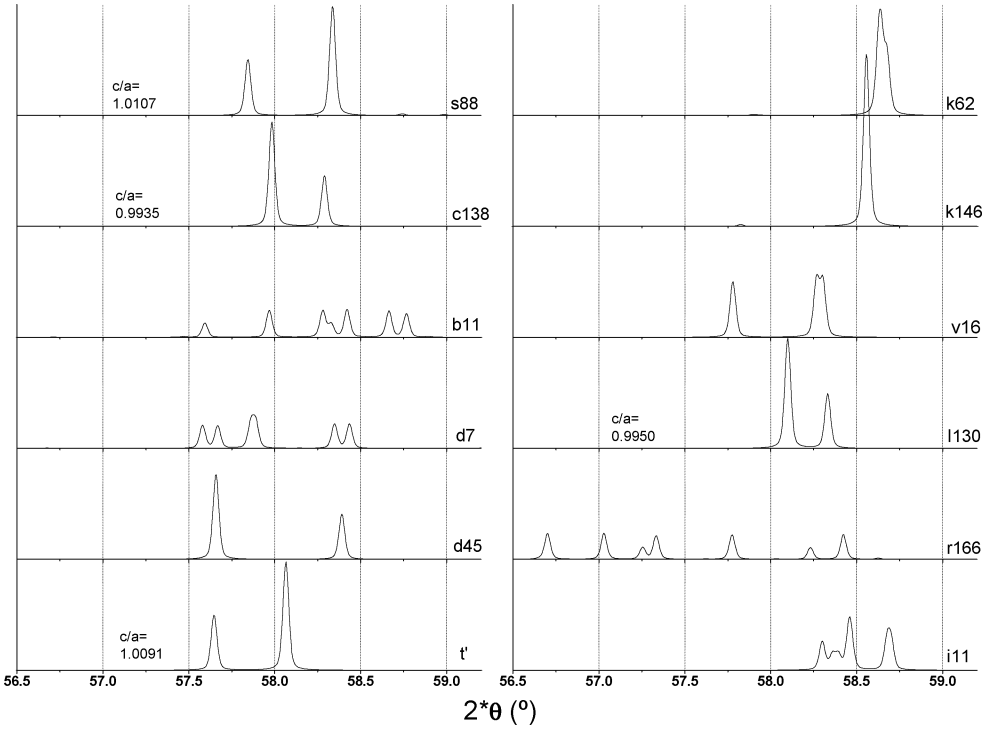

Figure 5. Cu Kα_1 powder XRD profiles, in the range corresponding to the (311) reflection of the fluorite lattice, computed (with broadening by a pseudo-Voigt line shape of 0.04° width) for DFT-relaxed $Ce_{0.5}Zr_{0.5}O_2$ structures. For comparison, the profile similarly computed for the structure obtained for a typical t′-type phase[10] is also plotted in the lower-left corner. Values of the tetragonality index (*c/a* ratio of the related near-cubic cell) are included in the tetragonal structures.

approximation, if rather than keeping constant the difference ΔC_p the ratio between both C_p values remained constant, from the enthalpy versus temperature relationship given for the monoclinic form in the same tables one would obtain similarly 12.62 kJ/mol for the tetragonal−monoclinic enthalpy difference at 0 K. As shown in Table 1, this value is approached rather better by the DFT method than by the atomistic one, showing that the quantum computation is more reliable also for estimating energy differences, at least for pure zirconia.

In view of the significant differences appearing between both sides of Figure 1, one must consider that, with the parameters available at present, the atomistic method will yield for CZMOs rather exaggerated lattice distortions and inaccurate energy differences; one should thus rely preferentially on the DFT results. Still, atomistic methods are of interest as they are much faster and thus allow to compute a larger number of structures and to identify negative phonon frequencies in reasonable time. Maybe this latter method could be made more accurate through an optimization of the energy parameters in it, for example, by fitting to DFT-computed energy hypersurfaces, or by including ion compressibility or quadrupole polarizability effects, which have been claimed to be important in such simulations.[55] This would be particularly convenient here; by combining a better accuracy with the ability to handle much larger unit cells, such atomistic calculations would allow to model more adequately solid solutions with true random cation distributions. The results could then be taken as reference basis for the discussion and evaluation of other features mentioned below (energetics of phase disproportionation, change in radial distribution functions upon ordering, etc.). With the now available parametrization, however, this would not be reliable. Apart from that, of course, using "averaged" cations, as done in some previous atomistic modelings in the literature,[29,30,31] would make impossible (even with a good initial parametrization) to reflect the significant differences in structure and energy that, as shown in this work, can appear because of different cation distributions and different ion displacement patterns originated by them.

Overall Trends in Zr−O Coordination and Energy Features of CZMOs. The next observation of interest arises from the overall features of the computed RDFs. As Figure 4 shows, the coordinations around Ce in the computed structures tend to be more regular than those around Zr. This is surely related to the larger radius of the Ce ion, which, by trying to achieve the most compact packing, determines to a large extent the cell dimensions and gets the most tight situation, while the smaller Zr and O ions have more room to move and to adjust positions so as to get the lowest energy. Of particular interest is the fact that the different cation orderings lead to rather different RDFs in the anion coordination sphere around Zr. This means that, in any situation where a real random solid solution is formed and in which therefore one can presume the coexistence of a large number of different mutual arrangements of Ce and Zr ions at the local level, many different distortions of the Zr coordination sphere will be present; the envelope of their RDFs is then expected to be rather broad and ill-defined. For such a situation, using only two anion shells when fitting Zr edge EXAFS data, as is the case in some of the recently published work,[27,32,28] may constitute a rather simplified approximation; in principle, a better description would be achieved using, for example, three-shell or four-shell models. Of course, using one of such more detailed models to analyze EXAFS data is admissible only if these latter contain enough information; it is well known that, because of Nyquist's theorem, this depends on the range of *k* and *R* values utilizable for the analysis.[56] Of the EXAFS works just mentioned, it seems clear that, at least in refs 27 and 32 (especially in the former), adding in the fitting a third O shell around Zr would probably be allowed by the *R* and *k* ranges used; it does not appear to be so in the work of ref 57, while in the case of ref 28 this is not so clear. Therefore, if a fitting with only two shells were clearly sufficient (i.e., if

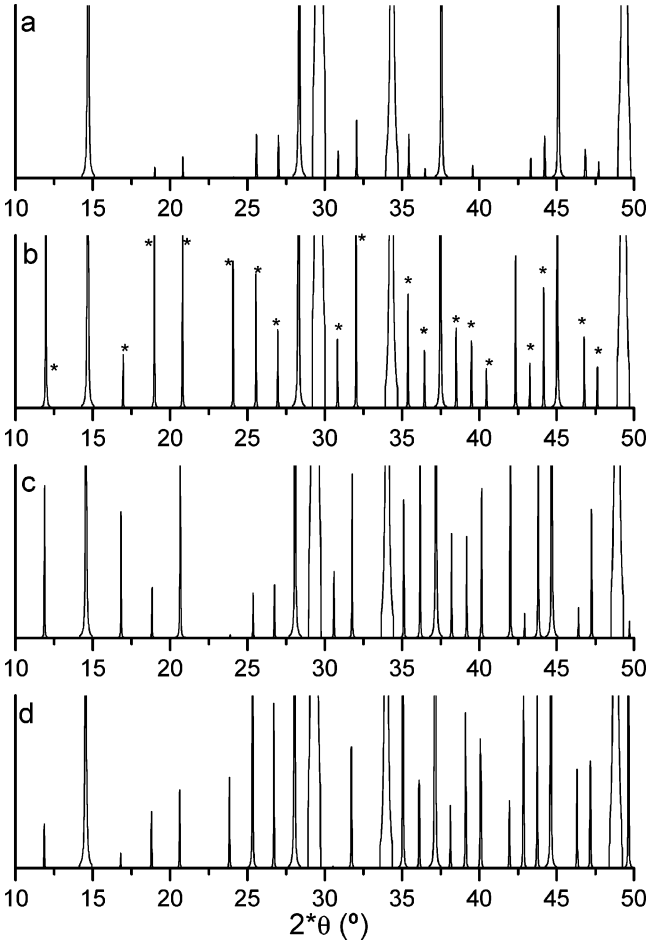

Figure 6. Cu Kα_1 powder XRD profiles computed, with broadening by a pseudo-Voigt line shape of 0.04° width, for κ-phase structures derived either from DFT calculations (a, b: **k**62 and **k**146 models, respectively) or from experimental data (c, from XRD results in ref 18; d, from neutron diffraction results, indicating the presence of Frenkel defects, in ref 20). The vertical scale, same in all plots, is chosen to better appreciate the lines (marked with asterisks) not allowed within the pyrochlore $Fd\bar{3}m$ symmetry.

no significant improvement in the fit were achievable by including a third shell) in some case in which a larger number of them was allowed by the data range collected, this would probably mean that in the material examined some specific cation ordering did exist, even if only at a relatively short range. Further comment on this is given later.

Now the energy values obtained can be discussed. Considering first the overall features, Table 1 shows that the atomistic calculations yield a considerably broader range of energies than the DFT-based ones. This is in line with the above-discussed difference between both methods when computing the differences in energy between the two ZrO_2 forms and might be related with the mentioned larger degree of lattice distortion which the first method tends to produce. An additional reason might be that the atomistic calculations use formal charges, so that the electrostatic interactions will be overemphasized. In any case, the first-principles DFT method should be considered a priori more reliable, even if it does not include dispersion (London type) interactions, that is, those which are included in the atomistic calculations through a C/r^6 term. In general, this term will produce a stabilization effect roughly proportional to the square of the density, so that structures with smaller molar volumes would be stabilized more. An estimate of the influence of these dispersion interactions on the DFT-derived energy values has been made by computing the contribution of that

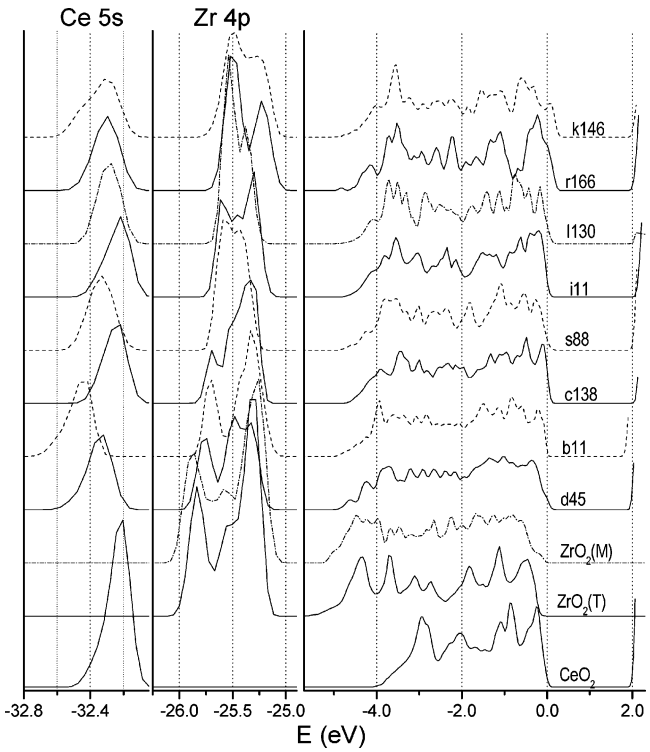

Figure 7. Density-of-state plots (broadened with a Gaussian of 0.03 eV width) obtained with DFT calculations; see text for details about the energy scale alignment. Right part: valence band and band gap regions. Left part: shallow (semicore) Ce(5s) and Zr(4p) levels.

C/r^6 term for each lattice (within the same geometries obtained by the DFT method and using the same C parameters as in the atomistic calculations). The results (not shown) do change somewhat the ordering of the different structures, but since the reliability of this procedure is doubtful they will not be considered further.

At this stage, therefore, one can state that the differences in energies among the various structures have magnitudes of ca. 10 kJ/mol or lower, that is, not higher than that between monoclinic and tetragonal zirconia, and that, while some orderings may be significantly preferred to others, still there are groups of them very similar in energy so that one can expect the coexistence of different mutual arrangements of Ce and Zr cations in real preparations and at normal temperatures.

Most Stable Configurations: Clustering versus Homogeneous Distribution of Cations. Looking now at the individual results, it is observed that both atomistic and DFT methods predict the lowest energy, among the structures examined, for a configuration of the double-layered **d** type. The relative order predicted for the other configurations varies from one calculation method to the other; if as said above one takes as more reliable the DFT data, one would conclude that the next most stable one is the **b** structure, followed by the **s**, **c**, and **i** structures (nearly equal in energy despite the rather different cation arrangement) and then by the (relatively complex) **f**2 and the single-layer ordered **l**130 type.

One may look for correlations between these energies and some structural factor, but this is not easy to achieve. For example, the evenness of the spatial distribution of both cations, and the degree of mutual interpenetration of their sublattices, could be thought to be a relevant factor. This can be somewhat measured by the N_{MM} parameter, given in Table 1; large values of it (and consequently low N_{CeZr} values) indicate an incomplete cation intermixing (i.e., clustering) and vice versa. It happens

that the most stable **d**-type has one of the highest N_{MM} values explored (8, with correspondingly $N_{MM} = 4$), and the next one (**b**11) has the highest one ($N_{MM} = 9$); however, of those immediately following in energy, the **s**-type presents just the opposite case ($N_{MM} = 4$, $N_{MM} = 8$), which also occurs for the **l**-type, while the intermediate value ($N_{MM} = N_{MM} = 6$) appears in the relatively stable **c** and **i** types and in most of all the other, less stable forms. Thus, on the basis of these results alone one cannot conclude the existence of a definite tendency favoring either high or low N_{MM} values.

In this point it is worth returning to the available EXAFS data. In the work by Nagai et al.,[27] the data obtained for a $Ce_{0.5}Zr_{0.5}O_2$ sample prepared by coprecipitation and calcined at 773 K indicated $N_{CeCe} = 8$ and $N_{CeZr} = 4$, thus coincident with the **d** case which appears here as most stable (and not too far from the $N_{CeCe} = 9$ situation presented by the **b** case, next in energy according to CASTEP). Also, in that work the O environment around Zr was fitted with two shells in a (6+2) pattern, which seems closer to the RDFs of the **d**- and **b**-type structures than to the (4+4) RDF patterns displayed by other low-energy structures with lower N_{MM} values such as those of **s, l**, or **m** type. Thus, it is possible that a structure of **d** or **b** type constitutes an acceptable representation of the local orderings dominating, at least, in that specimen. As pointed out in ref 27, the high N_{MM} value found in that case indicated the coexistence of regions more ZrO_2-like and with others more CeO_2-like; indeed, the **d** and **b** structures can be described as formed by stacking in an alternating manner two-layer-thick slabs (parallel to (100) and (111) planes, respectively) of both pure oxides. The fact that such topologies present lower energies in the present calculations is likely to be related to the way in which they facilitate the concerted displacement of (at least part of) the O ions and consequently optimize the Zr−O distances, but further insight in this respect is not obtained here.

From these considerations, one could conclude that a **d**- or **b**-type structure, with incipient separation of ceria and zirconia regions, might be present in the material studied in ref 27 and consequently also in other apparently homogeneous CZMO materials prepared in similar manner described in the literature. However, some discrepancies remain between the features of these structures and some of the available experimental data. First of all, while in ref 27 the EXAFS data at the Ce K edge were fitted with two cation neighbor shells having in total as expected 12 cations, in the Zr environment only the number of Ce neighbors was the expected one (i.e., nearly agreeing with the number of Zr neighbors around Ce); the number of Zr neighbors resulting from the fit was on the contrary rather low ($N_{ZrZr} = 3$), which suggests that the spread in Zr−Zr distances d(Zr−Zr) was rather large so that not all of them were captured by the EXAFS analysis. Now, the results (see Figure 4 for representative examples) show that, while indeed the spread in d(Zr−Zr) tends in general to be higher than that in d(Ce−Zr), reflecting the less tight placement of the smaller Zr ions in the lattice, for the **d**- and **b**-type structures analyzed this difference does not seem enough to explain the low value of N_{ZrZr} detected in those experiments. Second, to this author's knowledge electron microscopy observations of cell periodicity doublings in the [001] direction, as corresponds to the **d** topology, have not been reported in the literature; doubled interplanar spacing seems to have been detected only in the [111] direction (not conforming, thus, to the **b** topology, which implies a quadrupled periodicity) and this happened mainly in conditions compatible with the presence of the κ phase,[15,16] the structure of which does justify this type of doubling. These arguments thus indicate that if a definite cation ordering of Ce and Zr clustering type exists in these materials (even if apparently homogeneous) so as to lead to $N_{MM} > 6$, as found in ref 27, it might conform not to a **d**- or **b**-type double-layer pattern but to some other not considered here which, while allowing a high N_{MM} value, leads to a spread in d(Zr−Zr) rather higher than in d(Ce−Zr). Exploration of a much larger number of configurations may be needed to find a model satisfying all these requirements.

One has to consider also that different (apparently homogeneous) CZMO materials, prepared by different ways, may contain different cation distributions and lattice distortions. Indeed, for the material analyzed in ref 32, a (4+4)-type Zr−O coordination scheme was claimed from the EXAFS data, with a difference in Zr−O distances of ca. 0.25 Å (once anharmonicity in the second shell is taken into account via cumulant expansion), suggesting a structure significantly different from that in ref 27, 28, or 57. (However, there are discrepancies among these different authors concerning the EXAFS analysis methodology for the Zr−O shells. A critical examination of this issue, which depends critically on the source of the phaseshift functions, is not the role of the present work.) Of the structures obtained here with lower energies in the DFT calculations, such (4+4) coordination pattern is observed for the **s** and **l** topologies, and, to a lower extent, also for **i**11, although only in this latter does the split in Zr−O distances approach clearly the EXAFS-derived one. Now, one of the lower energy structures (**s**88) is, of all those studied here, the only one (besides **m**112, not shown in Figure 5 and approximately also **v**16) which clearly presents in its cell shape the same type of tetragonal character that is normally observed for the several phases (t, t′, t*, t_{meta}) reported in studies of homogeneous, well-crystallized $Ce_{0.5}Zr_{0.5}O_2$ materials, where typically ratios $c/a = 1.008-1.009$ are found.[14] All the other structures studied here present in the diffraction pattern either the opposite situation (i.e., $c/a < 1.000$) or no special tetragonal appearance. Therefore, considering the energy values obtained, the **s**-type structure, which as said above occurs for other chemically similar $MM'O_4$ double oxides involving heavy atoms of different sizes, might be an appropriate model for such situations.

At this point it is worth noting the EXAFS results obtained by Fornasiero et al.[28] for (Ce, Zr) mixed oxide materials of approximate composition $Ce_3Zr_2O_{10}$. Although the different Ce:Zr ratio does not permit a direct comparison with the results of the present calculations, it is remarkable that, for the two well-crystallized specimens studied there and which probably have some degree of cation ordering (in view of their Raman spectra, which were more complex than those of typical random solid solutions), the fitting of the EXAFS contributions of nearest cation neighbors around Zr led to N_{MM} values significantly below the figure ($N_{MM} = 4.8$) which would correspond to a purely random distribution of cations for that composition. Since at least one of these specimens displayed in the X-ray diffractogram a clearly tetragonal character (with $c/a = 1.003$, appropriate for this Ce/Zr ratio), a good concordance, at least in terms of general trend, with the **s**88 structure can be concluded. The lack of superstructure features in the diffraction patterns of these materials, even if they present cation ordering, may be due to insufficient dimension of the ordered domains; the coexistence of **s**88 structure microdomains having their *c* axes parallel would suffice to conserve the tetragonality. The symmetry of the **s**88 lattice (space group $I4_1/a$) is that which results when applying to the maximum symmetry of this cation ordering topology (the space group $I4_1/amd$) the same type of anion displacement along the *c* axis which when applied to the

fluorite lattice leads to the $P4_2/nmc$ symmetry of tetragonal zirconia, which is the symmetry normally ascribed to CZMO tetragonal phases. Indeed, the oxygen ions in the **s**88 structure obtained are all equivalent and displaced from the ideal fluorite positions (by ca. 0.23 Å) in directions which are closer to the *c* lattice vector (the angle formed by them with the latter is ca. 37°) than to the other lattice vectors ($I4_1/a$ is an immediate subgroup of $I4_1/amd$, i.e., the amount of symmetry decrease involved in the anion sublattice distortion is a minimal one). Perhaps the presence in this topology of a well-defined tetragonal direction facilitates the onset of this concerted anion movement, although this is not the only criterium of stability, since structure **m**112, which has also similar tetragonal character (as ascertained from the XRD simulation, not shown) and anion displacements, appears with much higher energy. Unfortunately, no other EXAFS data providing N_{MM} values have been published for well-crystallized CZMO tetragonal materials (the highly sintered ones studied in ref 27 correspond to the κ phase, and in other cases as those given in refs 46 and 57 for ratios Ce/Zr = 1.0 the random solution value, $N_{MM} = 6$, was kept fixed, not subjected to fitting). Additional information about (simultaneously) Zr−O coordination and N_{MM} values in these materials, which could clarify the situation, is therefore not available.

Thus, it seems plausible that different cation mutual distributions which may appear in CZMOs depending on preparation method and thermal treatment may be modeled by different structures of those examined here. In particular, the double-layer lattices **d** and **b** might be adequate models of cases containing some extent of cation clustering (including intermediate stages of the experimentally observed compositional disproportionations), while the **s** structure might represent tetragonal phases, especially if obtained in conditions favoring good homogeneity and cation ordering. Still, one must take into account also that even for one same cation ordering several energy minima may exist characterized by different ion displacement patterns, at least in some cases (see, e.g., the results for the **d**, **k**, and **l** types). It might be thus that the transformations between different tetragonal phases reported to occur at temperatures above 1173 K[14,10] correspond to transitions between such local minima. A careful EXAFS analysis of these phases would be therefore of great interest.

In any case, the data in Table 1 suggest that there is some energetic advantage in having, rather than a homogeneous cation distribution, ZrO_2-like domains coexisting with others CeO_2-like, which would thus justify the high N_{CeCe} values found by Nagai et al.[27] in their EXAFS data. This could be at the base of the known tendency of nearly equimolar ceria−zirconia mixed oxides to disproportionate in Ce-rich and Zr-rich domains, at least in small crystallite size samples where nucleation of new phases is easier.[23] Actually, the fact that for all the CZMO structures the CASTEP calculations yield $\Delta E > 0$ would imply that the completely disproportionated situation, that is, a mixture of both single oxides, is more favorable than any of the mixed structures; entropy and thermal effects, which may be relevant in real situations and are not taken into account here, could then lead at finite temperatures to a preferred situation with incompletely demixed phases.

A final word of caution should be given concerning the results obtained here: these apply in principle only to solids with well-developed crystalline particles. Indeed, for very small particles, with crystallite sizes of ca. 10 nm or below, it is known that the crystalline structures may present, for this type of materials, smaller symmetry distortions than those occurring for large crystallite sizes. Thus, for particle sizes below ca. 17 nm pure zirconia may present the tetragonal modification rather than the more stable monoclinic one,[58] and even a cubic symmetry might appear, as deduced from Raman data, for very incipient crystallization stages.[59] Also, as said in the Introduction section $Ce_{1-x}Zr_xO_2$ materials with $x > 0.4$ can present, if their particle sizes are small, the pseudo-cubic t″ phase rather than the real tetragonal form which is more stable for those compositions. Thus, comparing these calculations with experimental data obtained on high surface area, materials might be inadequate.

Structural Characteristics and Energetics of the κ Phase. A situation opposite to that described above for the **d**-type structure and the other low-energy forms discussed occurs in the **k** structure type, which represents the κ phase. Here, the cation ordering topology, which in the absence of distortions has an intrinsic cubic symmetry, provides no preferent directions for concerted anion movements. Anion displacements from the ideal fluorite positions are thus not particularly facilitated, leading to a relatively narrow distribution of Zr−O distances in the DFT-computed structure both for **k**62, derived from the GULP-optimized lattice, and for **k**146, obtained starting directly from the published structure (see Figure 1). This agrees with the EXAFS results obtained in ref 27 for a κ phase material, which could be fitted with a single Zr−O distance.

These simulation and EXAFS results, however, disagree with the Zr−O RDF profile resulting in the crystal structure which was reported for the κ phase in another work based on X-ray diffraction data[18] (Figures 1 and 4) and which reveals a quite nonuniform Zr−O coordination. It is remarkable that these latter results imply the presence of some Zr−O and Ce−O distances as short as 1.82 and 1.99 Å, respectively, which seem very short (especially the second one) if one compares them with those found experimentally for the pure single oxides and with the results of the DFT calculations. It seems probable that, if such structure had been present in the κ phase examined in ref 27, more than one Zr−O coordination shell would have been required for fitting its EXAFS data. Apart from this, one notes also that while the DFT simulations predict for both **k** models a configuration of Ce−Ce distances significantly more regular than that of the Zr−Zr pair, no such thing is observed in the RDFs (given in Figure 4) resulting from these diffraction-derived data.

The above-mentioned apparent conflict between two types of experimental data will have to be solved in future experimental works, paying particular attention not only to the data analysis procedures but also to the material preparation method, ensuring that the expected cation ordering has been produced and verifying, especially, whether some of the oxygen introduced during the reoxidation step remains in interstitial octahedral positions (Frenkel defects) as it has been found to occur in some cases.[13,19,20] Indeed, Mamontov et al.[22] claim that for CZMO such interstitial oxygen may remain in the reoxidized phase even after treatments of the latter up to 1050 K. This temperature was not reached during the preparation of the κ phase in either of the mentioned experimental works.[18,27] It may well be that the different experimental conditions used in each case lead to different amounts and arrangements of Frenkel defects, which will be reflected in these diffractogram details; indeed, Figure 6 shows that these are different in the cases described in refs 18 and 20. Furthermore, in ref 18 the fitting was carried out imposing cubic symmetry on the basis of the apparently cubic shape of the lattice; the latter, however, is compatible with a lower symmetry according to the present simulation results, as evidenced by the plots in Figure 5, and

indeed the deviation of the rombohedral angle in **k**146 from 90° turns out to be less than 0.001°. Considering the synthesis temperature, it may be that some anionic Frenkel defects were present also in the κ-type material examined by Nagai et al.,[27] but the degree to which they might affect the EXAFS results obtained there is unknown.

These considerations on the inappropriate use of cubic symmetry constraints during the fitting and on the possible presence of Frenkel defects imply that one must ascribe some uncertainty to the XRD-derived structure proposed in ref 18. The validity of the **k**-type structures obtained in the present work as models of the κ phase (at least when defect-free) cannot therefore be verified. The present simulations are however still valuable in indicating that the particular cation ordering in the κ phase does not favor significant deviations of the crystal cell from the cubic proportions (at least in the absence of Frenkel defects), even if lower symmetry exists at the local level.

Besides these structural indications, the present DFT calculations show for the κ phase models an excess energy ΔE significantly higher than that of the most stable structures (see Table 1 and Figure 2). This agrees with the observed fact that in the oxidized state this phase is clearly unstable. According to the work by Otsuka-Yao-Matsuo et al.,[14] the difference in Gibbs energy of formation $\Delta G°$ between this phase and the so-called t* phase, claimed by those authors to be one of the most stable homogeneous ones at low temperature, is estimated from emf measurements to be 22.3 kJ/mol (at $T = 0$ K). Although this value has a large uncertainty, being an extrapolation from data at $T > 873$ K, one notes that it is intermediate between those predicted by GULP and CASTEP for the difference in energy between the **k** and the lowest-energy **d** structures (Table 1). It seems likely that this high energy is due to the above-mentioned inadequacy of the cation ordering in this phase for favoring structure-stabilizing lattice distortions. In fact, in view of the published data which indicate that oxygen interstitials may remain in this material even after calcinations at 1050 K,[22] one may wonder whether the energy of the κ phase could be lower with these anion Frenkel defects than without them. A computational assessment of this point is however outside the possibilities of the present study because of the complexities introduced by fractional site occupation effects and the low reliability of the available atomistic model parametrization.

Electronic Structure Features. The results of the DFT calculations concerning electronic levels can be now examined to see if they afford some suggestions about other experimentally observable features which could be sensitive to different cation orderings. Overall, the results indicate relatively similar electronic characteristics for the different arrangements. Concerning the Mulliken analysis, it is well known that, although the absolute values derived from it are not reliable, the variations observed in them can still yield valuable insights. Here it has been noticed, as mentioned in the Results section, that there is some difference in Ce charges between a couple of structures (**k**62 and **l**130) and the rest. It might therefore be that different cation arrangements in CZMOs could lead in some case to differences in the Lewis acidity of these cations (when exposed at the surface), so that differences in vibration frequencies (measurable with IR spectroscopy) or adsorption strength (measurable, e.g., via thermal desorption) of adsorbed molecules could appear which could be used as fingerprint. It may well be that these differences are rather small, however, and that no clear information can be obtained in this way. There could be more significance in the differences in Ce(4f) orbital population values. It is generally admitted that the relatively complex shape (three spin−orbit doublets) of the 3d XPS spectra typically observed for the Ce^{4+} state in oxide-type compounds is related to a mixing of configurations ($4f^0L^n$ and $4f^1L^{n-1}$, where L^{n-1} indicates a hole in the ligand-derived valence band) in the initial state,[60,61] although the specific need of a mixed configuration description has been contended.[62] The relative positions and intensities of the three XPS doublets are related to the degree of configuration mixing, all of these factors depending on the relative strength of different electronic energy terms; thus, differences in electron density at the Ce(4f) orbitals such as those indicated by the Mulliken analysis in some cases might have consequences on the precise positions or intensities of the Ce 3d XPS peaks. It would be interesting to see if ceria−zirconia samples prepared in different ways show appreciable differences in these spectra. Still, one must note that, according to the calculations, this effect appears differently in the **k**62 and **k**146 structures, implying that it does not depend solely on the topology of cation ordering.

In respect to the energy levels derived from the DFT calculations, the DOS plots in Figure 7 provide some indications with possible practical interest. In the case of the deeper levels, small variations are observed in the energy of the Ce(5s) state; these should be interpreted actually as variations in the energy difference between the Ce(5s) and Zr(4s) level, as the latter was taken here (more or less arbitrarily) as reference. This means that, if one measures experimentally via photoemission spectroscopy the difference in position between those two levels, perhaps it might be possible to observe variations between differently prepared samples which are correlated to the cation distribution. This experiment is likely to require the use of synchrotron radiation; standard XPS would probably not have enough resolution for this. However, such experimental data are unlikely to be of much use, as a clear correlation between such variations and structure-related parameters is not apparent. For the Zr(4p) level, some differences appear in the peak shape; the energy interval spanned by it increases with N_{ZrZr}, which probably reflects the expected increase in the width of the corresponding electronic band with the increase in the number of overlaps among the constituent atomic orbitals. The study of the width and shape of this shallow band with (preferably ultraviolet) photoemission spectroscopy might therefore be useful in characterizing the degree of Zr−Zr clustering in these materials.

The DOS data obtained for the valence band region (right part of Figure 7) present some interesting features. On one hand, comparison of the bottom of the VB for the different materials indicates that its position is dominated by the extent of Zr−O interactions, which by allowing the appearance of shorter bond lengths can stabilize some valence O orbitals in the bonding region more than the Ce−O interactions. The width and overall profile of the band itself is not very different among the several CZMO structures displayed; however, for both **k** structures (and, to a smaller extent, also for **r**166) the top of the band appears at a significantly higher energy than for the rest, a fact that is not due simply to a bad alignment of energies once the positions of the other DOS features are considered. This suggests the existence of O-based levels of higher energy; it might be therefore that in a CZMO structured in this way the electron-donating capabilities were more important than in the rest. This is a surprising observation, since in one of these cases the Mulliken charge on Ce appears to be larger (vide supra). If such characteristics were kept by the atoms when at the surface, this could imply the simultaneous presence of stronger Lewis acid and basic sites in the κ phase.

Concerning the magnitude of the band gap found for these structures, it must be recalled that DFT is not reliable for the evaluation of that parameter. Indeed, LDA calculations normally underestimate it; here, with Ce(4f) levels present which will involve strong correlation effects, the problem may well be even larger. The band gap computed here for CeO_2, ca. 2.0 eV as shown in Figure 7, is accordingly rather lower than the real one, which lies around 3.0 eV[53,63] and leads to an absorption spectrum of CeO_2 that begins just at the end of the visible range and gives to this solid its light yellow color. Even if these calculations are not accurate, still they allow to make comparisons, and thus the results in Figure 7 indicate that the band gap in the majority of the mixed oxide structures studied is rather close to that of pure CeO_2. A quite significant exception is found with the **k**-type structures, for both of which the gap seems to be ca. 0.25 eV smaller. This latter difference agrees with experimental observations[18] reporting that the κ phase, modeled here by structures **k**, has a much more intense yellow color than the (more stable) tetragonal forms of this material, which indicates a more important light absorption in the upper visible range; the calculations presented here show that it is not necessary to invoke the presence of Frenkel defects (not included in the model) to explain this fact. Since the band gap computed for most of the other structures is quite closer to that obtained for CeO_2, one may suggest the use of the UV−vis absorption spectrum as a test of the presence in these materials of the κ phase or at least of local arrangements with similar characteristics as in the latter. On the other hand, since CeO_2 has proven to have a significant capability as photocatalyst when excited with near-UV radiation,[64,65] this result suggests that CZMOs with the κ phase structure might have relevant activity as photocatalysts within the upper range of the visible spectrum.

Conclusions

The study with atomistic and quantum methods of several ordered $Ce_{0.5}Zr_{0.5}O_2$ structures has allowed to verify several correlations and differences which lead to some interesting conclusions:

(1) The atomistic method, with the potentials and parameters used in the literature, is significantly less accurate than the DFT method in these modelizations. In particular, it tends to exaggerate the lattice distortions and the differences in structure and energy between different cation-ordering configurations. Even when computed with DFT methods, these latter differences may be important, implying that any approach using "averaged cations" within an atomistic calculation is likely to miss relevant effects at the local level.

(2) Different cation distributions will lead to significantly different Zr−O coordination patterns; this implies that a randomly disordered ceria−zirconia solid solution is likely to have a rather broad and ill-defined distribution of Zr−O distances. Any clear indication, for example, by EXAFS, of the presence of only one or two well-defined Zr−O coordination spheres could be thus an indication of the presence of specific cation orderings, at least at a local level.

(3) According to both types of calculation, the most stable structure among those examined is one based on alternating double layers of cations parallel to the (100) plane of the parent fluorite structure, leading to a high number N_{MM} (=8) of equal cation neighbors; the latter value coincides with recent EXAFS data obtained on a low particle size material, which also show a (6+2) Zr−O coordination pattern compatible with the results of the simulations of this layered structure. A structure having also double-cation layers, but with these oriented parallel to the (111) plane, and which has also a high N_{MM} (=9), would be the closest one in energy according to the DFT calculation. Such lower energies may be related to the facilities for concerted anion displacement provided by such extended clustering and ordering of Zr cations and might be at the origin of the disproportionation into Zr-rich and Ce-rich phases experimentally observed to occur upon thermal treatments in ceria−zirconia specimens of catalytic grade.

(4) A tetragonal crystalline form with $c/a > 1.00$, that is, like that normally found in the more stable forms (t′, t*, and others) of well-crystallized Ce−Zr oxides, does not appear in any of these double-layered structures. It occurs, however, in one of the slightly more energetic structures (the **s** type), which, in contrast with the double-layered ones, is characterized by rather low N_{ZrZr} values. Low N_{ZrZr} values have been reported in EXAFS analyses at least in one case[28] in which this tetragonal character of the unit cell could be verified by diffraction. Therefore, the **s**-type structure, adopted also by related mixed oxide compounds such as $HfGeO_4$, $CeGeO_4$, $LaNbO_4$, and several other $MM'O_4$ oxides[66] (and which may facilitate also concerted anion movement along a preferred fluorite axis), or some related one, could be a good model for $Ce_{0.5}Zr_{0.5}O_2$ materials which have not developed cation-clustering characteristics. A Zr−O coordination pattern of (4+4) type is predicted for this structure. Although such pattern has been claimed to appear in other work on this type of materials,[32] it is in disagreement with the EXAFS analysis reported in ref 28; given the controversy existing on the methodology of these analyses, a critical appraisal of this discrepancy cannot be made here.

(5) The energy differences between some of these structures are modest (a few kcal/mol); it may well be therefore that very different cation arrangements can appear in this type of mixed oxides, being conditioned largely by the preparation method. The N_{MM} values, accessible via EXAFS measurements and perhaps also (to some extent) through photoemission spectroscopy, may serve to characterize different situations in this respect. Such EXAFS data, coupled with Raman results, might help also to clarify the nature of the differences between the several tetragonal structures (t′, t*, and so forth) reported in the literature.

(6) The κ phase of $Ce_{0.5}Zr_{0.5}O_2$, which can be obtained by controlled oxidation of the pyrochlore compound $Ce_2Zr_2O_7$ and has with all probability the same cation ordering as this latter, is predicted to be highest in energy among those examined, in agreement with its known metastable character. While experimental data suggest for this phase a cubic structure, the calculations indicate for it a lower (possibly rombohedral) symmetry but with nearly cubic unit cell proportions and rather uniform Zr−O coordination distances. The latter agree with EXAFS results reported for this phase but not with the crystal structure derived in the literature from diffraction data; a reexamination of these latter experimental data considering a crystal symmetry lower than cubic, with attention to the possible presence of interstitial anions in the structure (Frenkel defects), could therefore be of interest.

(7) The electronic structure calculations carried out for the κ phase suggest that there might be differences in acid−base character in comparison with the other structures. More interestingly, they predict also a smaller band gap, in agreement with the more intense yellow color experimentally observed for this material; this latter characteristic might lead to photocatalytic activity in the visible light range.

Acknowledgment. Financial support by CICYT (project MAT2000-1467) is acknowledged. Thanks are given to J.D.

Gale for kindly providing the GULP program, to the Centro Técnico de Informática del C.S.I.C. for access to computing facilities, and to one referee for several suggestions which were useful for the final manuscript form.

Supporting Information Available: Supporting Information is provided giving the crystal structures of the mixed oxide lattices as optimized by CASTEP. This material is available free of charge via the Internet at http://pubs.acs.org.

References and Notes

(1) (a) Ozawa, M.; Kimura, M.; Isogai, A. *J. Alloys Compd.* **1993**, *193*, 73. (b) Murota, T.; Hasegawa, T.; Azoasa, S.; Matsui, H.; Motoyama, M. *J. Alloys Compd.* **1993**, *193*, 289.

(2) Ranga Rao, G.; Kašpar, J.; Meriani, S.; di Monte, R.; Graziani, M. *Catal. Lett.* **1994**, *24*, 107.

(3) Kašpar, J.; Fornasiero, P.; Graziani, M. *Catal. Today* **1999**, *50*, 285.

(4) Kawamura, K.; Watanabe, K.; Hiramatsu, T.; Kaimai, A.; Nigara, Y.; Kawada, T.; Mizusaki, J. *Solid State Ionics* **2001**, *144*, 11.

(5) Wang, S.; Lu, G. Q. *Appl. Catal., B* **1998**, *19*, 267.

(6) Montoya, J. A.; Romero-Pascual, E.; Monzón, A.; Guimon, C. *Stud. Surf. Sci. Catal.* **2000**, *130D*, 3669.

(7) Putna, E. S.; Vohs, J. M.; Gorte, R. J. *Catal. Lett.* **1997**, *45*, 143.

(8) Yashima, M.; Morimoto, K.; Ishizawa, N.; Yoshimura, M. *J. Am. Ceram. Soc.* **1993**, *76*, 1745.

(9) Yashima, M.; Sasaki, S.; Yamaguchi, Y.; Kakihana, M.; Yoshimura, M.; Mori, T. *Appl. Phys. Lett.* **1998**, *72*, 182.

(10) Omata, T.; Kishimoto, H.; Otsuka-Yao-Matsuo, S.; Ohtori, N.; Umesaki, N. *J. Solid State Chem.* **1999**, *147*, 573.

(11) Yashima, M.; Arashi, H.; Kakihana, M.; Yoshimura, M. *J. Am. Ceram. Soc.* **1994**, *77*, 1067.

(12) McClellan, K. J.; Xiao, S.-Q.; Lagerlof, K. P. D.; Heuer, A. H. *Philos. Mag. A* **1994**, *70*, 185.

(13) Thomson, J. B.; Robert Armstrong, A.; Bruce, P. G. *J. Am. Chem. Soc.* **1996**, *118*, 11129.

(14) Otsuka-Yao-Matsuo, S.; Izu, N.; Omata, T.; Ikeda, K. *J. Electrochem. Soc.* **1998**, *145*, 1406.

(15) Vidal, H.; Bernal, S.; Kašpar, J.; Pijolat, M.; Perrichon, V.; Blanco, G.; Pintado, J. M.; Baker, R. T.; Colón, G.; Fally, F. *Catal. Today* **1999**, *54*, 93.

(16) Masui, T.; Ozaki, T.; Adachi, G.; Kang, Z.; Eyring, L. *Chem. Lett.* **2000**, 840.

(17) Otsuka-Yao-Matsuo, S.; Omata, T.; Izu, N.; Kishimoto, H. *J. Solid State Chem.* **1998**, *138*, 47.

(18) Kishimoto, H.; Omata, T.; Otsuka-Yao-Matsuo, S.; Ueda, K.; Hosono, H.; Kawazoe, H. *J. Alloys Compd.* **2000**, *312*, 94.

(19) Mamontov, E.; Egami, T.; Brezny, R.; Koranne, M.; Tyagi, S. *J. Phys. Chem. B* **2000**, *104*, 11110.

(20) Thomson, J. B.; Robert Armstrong, A.; Bruce, P. G. *J. Solid State Chem.* **1999**, *148*, 56.

(21) Tolla, B.; Demourgues, A.; Isnard, O.; Menetrier, M.; Pouchard, M.; Rabardel, L.; Seguelong, T. *J. Mater. Chem.* **1999**, *9*, 3131.

(22) Mamontov, E.; Egami, T.; Brezny, R.; Koranne, M.; Tyagi, S. *J. Phys. Chem. B* **2000**, *104*, 11110.

(23) Colón, G.; Pijolat, M.; Valdivieso, F.; Vidal, H.; Kašpar, J.; Finocchio, E.; Daturi, M.; Binet, C.; Lavalley, J. C.; Baker, R. T.; Bernal, S. *J. Chem. Soc., Faraday Trans.* **1998**, *94*, 3717.

(24) Fornasiero, P.; Balducci, G.; Di Monte, R.; Kašpar, J.; Sergo, V.; Gubitosa, G.; Ferrero, A.; Graziani, M. *J. Catal.* **1996**, *164*, 173.

(25) Baker, R. T.; Bernal, S.; Blanco, G.; Cordón, A. M.; Pintado, J. M.; Rodríguez-Izquierdo, J. M.; Fally, F.; Perrichon, V. *Chem. Commun.* **1999**, 149.

(26) Fornasiero, P.; Montini, T.; Graziani, M.; Kašpar, J.; Hungría, A. B.; Martínez-Arias, A.; Conesa, J. C. *Phys. Chem. Chem. Phys.* **2002**, *4*, 149.

(27) Nagai, Y.; Yamamoto, T.; Tanaka, T.; Yoshida, S.; Nonaka, T.; Okamoto, T.; Suda, A.; Sugiura, A. *Catal. Today* **2002**, *74*, 225.

(28) Fornasiero, P.; Fonda, E.; Di Monte, R.; Vlaic, G.; Kašpar, J.; Graziani, M. *J. Catal.* **1999**, *187*, 177.

(29) Balducci, G.; Kašpar, J.; Fornasiero, P.; Graziani, M.; Islam, M. S.; Gale, J. D. *J. Phys. Chem. B* **1997**, *101*, 1750.

(30) Balducci, G.; Kašpar, J.; Fornasiero, P.; Graziani, M.; Islam, M. S. *J. Phys. Chem. B* **1998**, *102*, 557.

(31) Balducci, G.; Islam, M. S.; Kašpar, J.; Fornasiero, P.; Graziani, M. *Chem. Mater.* **2000**, *12*, 677.

(32) Lemaux, S.; Bensaddik, A.; van der Eerden, A. M. J.; Bitter, J. H.; Koningsberger, D. C. *J. Phys. Chem. B* **2001**, *105*, 4810.

(33) Gale, J. D. *J. Chem. Soc., Faraday Trans.* **1997**, *93*, 629.

(34) Conesa, J. C. *Surf. Sci.* **1995**, *339*, 337.

(35) (a) Ewald, P. P. *Ann. Phys.* **1921**, *64*, 253. (b) Tosi, M. P. *Solid State Phys.* **1964**, *16*, 1.

(36) Dick, B. G.; Overhauser, A. W. *Phys. Rev.* **1958**, *112*, 90.

(37) *Cerius2 v. 4.2 Users Guide*, Molecular Simulations Inc.: San Diego, CA, 2000.

(38) Payne, M. C.; Teter, M. P.; Allan, D. C.; Arias, T. A.; Joannopoulos, J. D. *Rev. Mod. Phys.* **1992**, *64*, 1945.

(39) Vanderbilt, D. *Phys. Rev. B* **1990**, *41*, 7892.

(40) Perdew, J. P.; Zunger, A. *Phys. Rev. B* **1981**, *23*, 5048.

(41) (a) Perdew, J. P.; Wang, Y. *Phys. Rev. B* **1992**, *46*, 6671. (b) White, J. A.; Bird, D. M. *Phys. Rev. B* **1994**, *50*, 4954.

(42) Francis, G. P.; Payne, M. C. *J. Phys. Condens. Matter* **1990**, *2*, 4395.

(43) Sánchez-Portal, D.; Artacho, E.; Soler, J. M. *Solid State Commun.* **1995**, *95*, 685.

(44) Segall, M. D.; Pickard, C. J.; Shah, R.; Payne, M. C. *Mol. Phys.* **1996**, *89*, 571.

(45) Mather, G. C.; Dussarrat, C.; Etourneau, J.; West, A. R. *J. Mater. Chem.* **2000**, *10*, 2219.

(46) Vlaic, G.; Fornasiero, P.; Geremia, S.; Kašpar, J.; Graziani, M. *J. Catal.* **1997**, *168*, 386.

(47) Bertaut, F.; Durif, A. *Comptes Rendus Acad. Sci.* **1954**, *238*, 2173.

(48) Ennaciri, A.; Kahn, A.; Michel, D. *J. Less-Common Met.* **1986**, *124*, 105.

(49) David, W. I. F. *Mater. Res. Bull.* **1983**, *18*, 749.

(50) Kümmerle, E. A.; Heger, G. *J. Solid State Chem.* **1999**, *147*, 485.

(51) McMullough, J. D.; Trueblood, K. N. *Acta Crystallogr.* **1959**, *12*, 507.

(52) Malek, J.; Benes, L.; Mitsusashi, T. *Powder Diffr.* **1997**, *12*, 96.

(53) Wuilloud, E.; Delley, B.; Schneider, W.-D.; Baer, Y. *Phys. Rev. Lett.* **1984**, *53*, 202.

(54) Chase, M. W., Jr. *NIST-JANAF Thermochemical Tables*, 4th ed.; J. Phys. Chem. Ref. Data, Monograph 9; American Chemical Society: Washington, DC; American Institute of Physics: Woodbury, NY, 1998.

(55) Wilson, M.; Exner, M.; Huang, Y.-M.; Finnis, M. W. *Phys. Rev. B* **1996**, *54*, 15683.

(56) Stern, E. A. *Phys. Rev. B* **1993**, *48*, 9825.

(57) Vlaic, G.; Di Monte, R.; Fornasiero, P.; Fonda, E.; Kašpar, J.; Graziani, M. *J. Catal.* **1999**, *182*, 378.

(58) Chaterjee, A.; Pradhan, S. K.; Datta, A.; De, M.; Chakravorty, D. *J. Mater. Res.* **1994**, *9*, 263.

(59) (a) Phillippi, C. M.; Mazdiyasni, K. S. *J. Am. Ceram. Soc.* **1971**, *54*, 254. (b) Berry, F. J.; Skinner, S. J.; Bell, I. M.; Clark, R. J. H.; Ponton, C. B. *J. Solid State Chem.* **1999**, *145*, 394.

(60) Fujimori, A. *Phys. Rev. B* **1983**, *28*, 2281.

(61) Kotani, A.; Parlebas, J. C. *J. Phys. (Paris)* **1985**, *46*, 77.

(62) Kaindl, G.; Wertheim, G. K.; Schmiester, G.; Sampathkumaran, E. V. *Phys. Rev. Lett.* **1987**, *58*, 606.

(63) Izaki, M.; Saito, T.; Chigane, M.; Ishikawa, M.; Katayama, J.; Inoue, M.; Yamashita, M. *J. Mater. Chem.* **2001**, *11*, 1972.

(64) Bamwenda, G. R.; Sayama, K.; Arakawa, H. *Chem. Lett.* **1996**, *30*, 157.

(65) Coronado, J. M.; Maira, A. J.; Martínez-Arias, A.; Conesa, J. C.; Soria, J. *J. Photochem. Photobiol., A* **2002**, *150*, 219.

(66) Depero, L. E.; Sangaletti, L. *J. Solid State Chem.* **1997**, *129*, 82.